Improved Prediction of Shrinkage Defects in SGI Castings Considering Expansion / Contraction Behavior and Mold Characteristics

Yutaka Miyamoto
Ube Steel Co., Ltd., Ube, Japan

Jun Sasaki
Daihatsu Metal Co., Ltd., Izumo, Japan

Takeshi Nakano
Tsuchiyoshi Industry Co., Ltd., Hiroshima, Japan

Haruki Itofuji
I2C Technology Institute, Ube, Japan

ABSTRACT

The expansion and contraction behavior of spheroidal graphite cast iron as it solidifies and the characteristics of silica sand, artificial sand, raw molds, and permanent molds were organized to improve the prediction accuracy of the shrinkage porosity. The expansion and contraction behavior during solidification was based on the method considered in the authors' previous research.[1] Mold characteristics, mold strength, thermal expansion coefficient of casting sand, and dimensions of castings were investigated, and the effects of mold movement during solidification on the amount of expansion and shrinkage were discussed. Based on the results, the expansion and contraction behaviors were calculated considering the mold characteristics, and shrinkage porosity was predicted by casting simulation. The resulting shrinkage cavity distribution was close to that of actual castings. And the possibility of improving shrinkage cavity prediction was found.

Keywords: spheroidal graphite iron, SGI, castings, simulation, shrinkage, artificial sand, green sand, permanent mold

INTRODUCTION

The expansion and contraction behavior of spheroidal graphite cast iron during solidification is modeled by segmenting the total shrinkage due to austenite crystallization and the total expansion due to graphite crystallization into discrete steps.[1] This method, applied by the authors in a casting simulation, allows for a more accurate reproduction of the actual solidification process compared to conventional prediction methods. However, the propensity for shrinkage cavities is influenced by mold characteristics. To further enhance prediction accuracy, factors such as mold strength, thermal expansion of the sand, and mold shape must be considered.[2-4] For instance, green sand molds are prone to external shrinkage, whereas metal molds typically do not exhibit external shrinkage unless they are unclamped. Regarding thermal expansion, external shrinkage cavities occur when artificial sand is used in the molds due to its low coefficient of thermal expansion. Additionally, the likelihood of internal shrinkage cavities decreases with a larger casting modulus and more cube-like shapes.

In this study, these mold characteristics were incorporated into the analysis of expansion and contraction behavior to further improve the accuracy of shrinkage cavity predictions.

EXPERIMENTAL PROCEDURE

LARGE CUBIC-SHAPED CASTINGS USING FURAN SELF-HARDENING MOLDING WITH EITHER ARTIFICIAL SAND OR SILICA SAND

The casting design, as shown in Figure 1, involved cubes with each side measuring 600 mm and a casting modulus of 10 cm. Two gates, each with a cross-section of 50 x 75 mm, were placed in the mold, and four flow-offs with a diameter of 60 mm were set on the upper mold face. The molds, made from either silica sand or artificial sand, were prepared to confirm shrinkage cavities and measure the cooling curve. The silica sand mold consisted of recycled silica sand, 0.8 wt.% resin, and 40 wt.% catalyst, while the artificial sand molds used mullite-based artificial sand, 1.4 wt.% resin, and 40 wt.% catalyst. An alcohol MgO-based mold wash was applied to the mold surface. A 10-ton low-frequency induction furnace was utilized for melting, with returned scrap and steel scrap serving as charge materials. After melting, the chemical composition was adjusted, superheating was conducted at over 1500C (2732F) for 5 minutes, and the molten metal was tapped following natural cooling. In sequence, 1.2 wt.% Fe-45mass%Si-5.5mass%Mg alloy was used as a spheroidizer, 0.3 wt.% Fe-75mass%Si alloy as an

inoculant, and 2.0 wt.% punching scraps from electromagnetic steel sheets as cover material, were all placed in the ladle. The solidification curve was measured using a ⌀0.3 mm K-type thermocouple sheathed with ⌀1.6 mm Inconel, inserted into a ⌀5.0 mm outer diameter and ⌀3.0 mm inner diameter silica tube. The thermocouples were then positioned at the center of the casting's thickness.

SMALL CUBIC AND FLAT SHAPE CASTINGS USING GREEN SAND MOLDING WITH SILICA SAND

Figure 2 shows the casting design. The castings were shaped as a cube with each side measuring 70 mm, and as a plate with dimensions of 45 mm in height, 100 mm in length, and 100 mm in width. The casting modulus was approximately 1 cm. The molds, made of green sand, were prepared in two types: one for checking shrinkage cavities and the other for measuring the cooling curve. The green sand molds were composed of 3.0 wt.% moisture content and had a compactness value (CB) value of 40. A 30 kg high-frequency induction furnace was used for melting, with pig iron serving as the charge material. After melting, the chemical composition was adjusted, the molten metal was tapped, and Mg treatment was performed in a ladle.

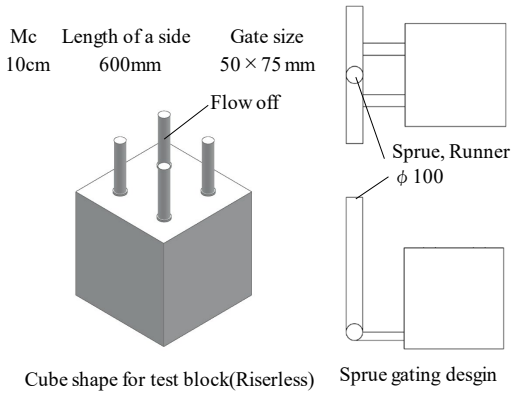

(a) Mold with Silica sand

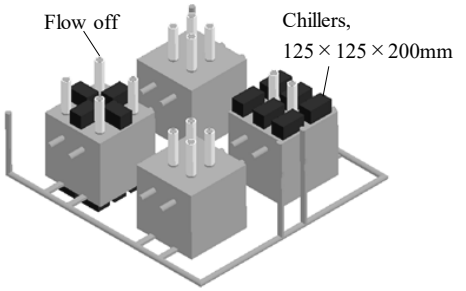

(b)Mold with artificial sand

Figure 1. Casting designs for a large cubic shape casting.

COIN SHAPE AND STEERING KNUCKLE CASTING WITH PERMANENT MOLD

Figure 3 shows the casting designs. The coin-shaped casting has a diameter of 37 mm and a thickness of 5.4 mm, with a casting modulus of 0.27 cm. The steering knuckle casting weighs 4.6 kg. The molds were made using SAE 1049 material and coated with a two-layer mold wash. The first layer consisted of acetylene soot, while the second layer was a diatomite system. The molds were preheated to 350C (662F). The melting and pouring conditions, as well as the cooling curve measurements, were conducted as previously reported.[5]

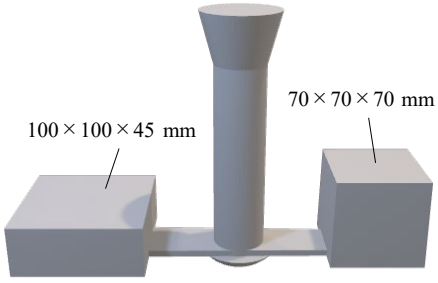

Figure 2. Casting design for small cubic and flat shape casting.

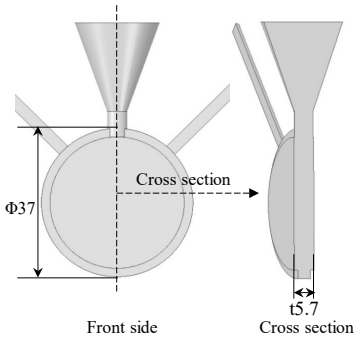

(a) Coin shape casting

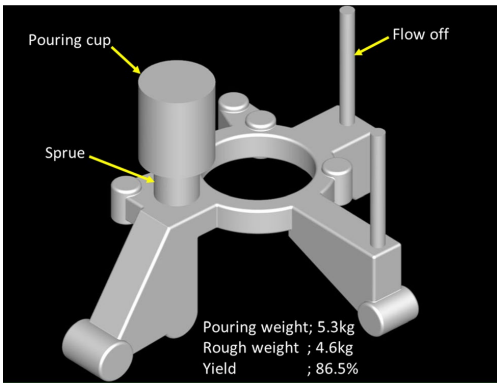

(b) Knuckle shape casting

Figure 3. Casting design for coin shape and steering knuckle shape casting.

SHRINKAGE CAVITY ANALYSIS

The expansion and contraction behavior during solidification was calculated using the chemical composition and cooling curves. First, the proportion of the reaction time in the total solidification time was obtained. The reactions occurring from the beginning of pouring to the end of the solidification were in the following order: 1) liquid contraction, 2) proeutectic reaction and liquid contraction, 3) liquid contraction 4) eutectic reaction, and 5) austenite contraction among the eutectic crystal cells. The start and end points of each reaction were determined by reading the inflection points in the measured solidification curve. The tangent method was adopted to determine the inflection point, and the percentage of the reaction was calculated assuming that the solidification ratio of 0.0% is at the finish point of pouring and at the starting point of solidification also, as shown in Fig. 4. Measurement for inflection point can also use the first derivative curve. Subsequently, the theoretical volume change was calculated by substituting the amount of carbon/silicon and the initial temperature of the cast at the end of the casting into Eqn.1.[2]

$$TV = Sl + Epg(or\ Sp\gamma) + Eeg + Se\gamma \qquad \textbf{Eqn. 1}$$

Where:
TV = volumetric change,
Sl = liquid shrinkage (vol %),
Epg = expansion of proeutectic graphite (vol %),
Spγ = contraction of proeutectic austenite (vol %),
Eeg = expansion of eutectic graphite (vol %), contraction of eutectic austenite (vol %)

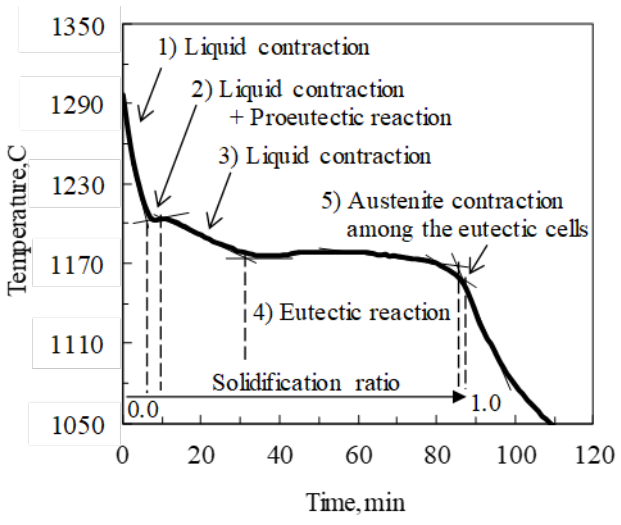

Figure. 4 Inflection points were determined by a tangent-line method and solidification ratio were determined for each point, for example.

In Equation 1, Epg was used when the chemical composition was hypereutectic and Spγ was used when the composition was hypoeutectic. These values may be determined by the following equations:

$$Sl = \left[\frac{(Ti-1423)}{100}\right] \times 1.5 \qquad \textbf{Eqn. 2}$$

$$Epg = \left[\frac{(Cx-Ce)}{(100-Ce)}\right] \times 3.4 \times 100 \qquad \textbf{Eqn. 3}$$

$$Sp\gamma = -3.5 \times \left[\frac{(Ce-Cx)}{(Ce-C\gamma)}\right] \qquad \textbf{Eqn. 4}$$

$$Eeg = \left[\frac{(1-Sl)}{100}\right] \times \left[\frac{(100-Cx)}{(100-Ce)}\right] \times \left[\frac{(Ce-C\gamma)}{(100-C\gamma)}\right] \times 3.4 \times 100 \qquad \textbf{Eqn. 5}$$

$$Se\gamma = -3.5 \times 100 \times \left[\frac{(1-Sl)}{100}\right] \times \left[\frac{(100-Cx)}{(100-Ce)}\right] \times \left[\frac{(100-Ce)}{(100-C\gamma)}\right] \qquad \textbf{Eqn. 6}$$

Where:
Ti = Initial temperature of molten metal in mold (C),
Ce = Carbon content at the eutectic point (mass%),
Cx = Carbon content of the molten metal (mass%),
Cγ = Carbon solid solution content in austenite (mass%),
3.5 = Shrinkage ratio of austenite,
3.4[1] = Density ratio of austenite/graphite

Here, the liquid contraction was assumed to be 1.5 vol% per 100 C.[6-9] Other equations used the lever rules in the equilibrium state diagram.
Furthermore, Ce and Cγ were determined by the following equations:

$$Ce = 4.27 + \frac{Si}{3} \qquad \textbf{Eqn. 7}$$

$$C\gamma = 2.045 - 0.178 \times Si \qquad \textbf{Eqn. 8}^{10}$$

Where:
Si = Silicon content in the molten metal (mass%)

Finally, the amount of expansion/contraction in each reaction was divided by the ratio of the corresponding reaction to calculate the degree of expansion/contraction. Hence, the expansion/contraction behavior was quantified. The actual calculation results will be shown later. The expansion and contraction behavior during solidification was adjusted according to the mold properties. For furan molds with silica sand, the thermal expansion coefficient of the silica sand was modified to subtract 0.5 to 1.0% from the liquid contraction value. In the case of green sand molding with silica sand, the expansion due to eutectic graphite during solidification was set to zero. It was assumed that the mold strength of green sand molds is low, and the expansion was absorbed by mold wall movement. Additionally, it was assumed that no thermal expansion of the silica sand occurred due to the high-water content in the green sand molds, which likely prevents a significant increase in mold temperature.

For permanent molds, the expansion due to eutectic graphite is considered negligible when the casting modulus is small. This is because graphite crystallizes within the numerous Mg bubbles present in the molten metal, and it is assumed that the graphite does not grow larger than these bubbles. Additionally, it was also assumed that no intercellular austenite shrinkage occurs when the casting modulus exceeds 1 cm, as eutectic expansion during solidification is believed to crush internal shrinkage cavities. The casting simulation software was used to apply the calculated values for expansion and contraction behavior to the solidification analysis. The physical property values used in the casting simulation are listed in Table 1. The green sand mold was configured to switch between two physical properties as the temperature increased: SAE 1049 properties up to a mold temperature of 300C (572F), and green sand properties at temperatures above 300C (572F). This setup was designed to account for the evaporation of water on the mold surface. Special values were assigned for the thermal conductivity of the green sand molds, while other values remained general. Element partitioning was performed to ensure that thicknesses were divided into three or more parts.

Table 1. Physical Properties for Simulation

	Casting	Chiller
Density (kg/m^3)	7000	7850
Specific heat (kJ/(kg·K))	1.047	0.670
Thermal conductivity（W/(m·K))	20.93	33.49

	Mold			
	Silica	Artificial sand	Greensand	SAE1049
Density (kg/m^3)	1550	1700	1500	7840
Specific heat (kJ/(kg·K))	1.047	1.84	1.051	0.486
Thermal conductivity（W/(m·K))	1.05	0.56	0.82	50.69

Heat transfer coefficient (W/(m^2·K))	Casting / Mold : 4186.2 Casting / Chiller : 1395.4 Mold / Chiller : 8372.4

EXPERIMENTAL RESULTS AND DISCUSSION

CASTING OF BLOCKS

Chemical composition and cooling curve

Table 2 shows the chemical composition of the casting blocks, and Figure 5 shows the cooling curves which were poured without any issues. The Mg yield is lower than the other castings value for the coin and knuckle castings. Although, this is on target and not a problem. As shown in Figure 6, the graphite was spheroidized and chill was not observed. The carbon equivalent (CE) based on industrially produced spheroidal graphite cast irons, with a hypoeutectic composition for large castings to control graphite dross and a hypereutectic composition for small castings and mold castings because graphite dross formation is not a consideration.

Table 2. Chemical Composition of Test Blocks (mass%)

Castings	C	Si	Mn	P	S	Mg	CE
Large (Furan, Silica)	3.25	2.31	0.26	0.052	0.010	0.048	4.02
Large (Furan, Artificial)	3.47	2.40	0.23	0.044	0.012	0.048	4.27
Small (Green, Silica)	3.68	2.24	0.27	0.020	0.010	0.037	4.42
Coin (Permanent)	3.44	3.22	0.06	0.019	0.013	0.016	4.51
Knuckle (Permanent)							

Expansion and contraction behavior

Table 3 shows the expansion and contraction values during solidification. Figure 7 illustrates the shrinkage behavior during solidification, with the horizontal axis representing the solidification ratio and the vertical axis indicating the degree of expansion and contraction. These values were calculated using the chemical composition and cooling curves discussed in the previous section and were subsequently adjusted to reflect the characteristics of each mold.

COMPARISON OF ACTUAL AND PREDICTED SHRINKAGE OCCURRENCES

Large cubic-shaped castings using furan self-hardening molding with artificial sand or silica sand

Figure 8 shows the results of the large cubic-shaped castings. For molds using artificial sand, external shrinkage was observed in the flow-offs and top surfaces. However, no internal shrinkage cavities were detected in the center of the casting. When a chill was installed on the cope, the degree of external shrinkage varied depending on the flow-offs and the number of chills used. In molds using silica sand, no external shrinkage cavities were observed on the flow-offs and top surface, and no internal shrinkage cavities were found in the center of the casting.

Figure 9 shows the predicted results of shrinkage cavities. As a result of the CAE analysis, the colored areas represent the degree of surface shrinkage and depression on the cope face, as well as inner shrinkage in the section. The gray boxes indicate that no shrinkage was detected in the CAE analysis results. For molds using artificial sand, external shrinkage was indicated as observed in the actual castings. For the silica sand mold, the results considering its thermal expansion were closer to the actual shrinkage cavity distribution.

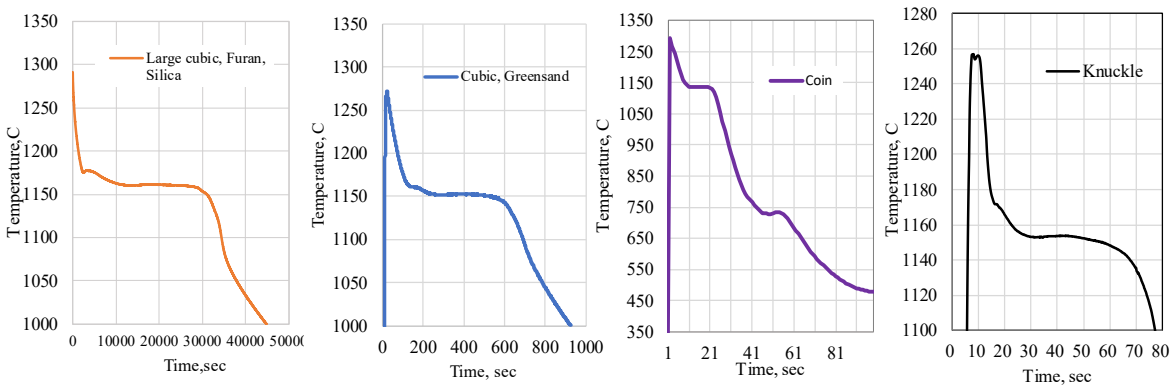

Figure 5. Cooling curves of the castings.

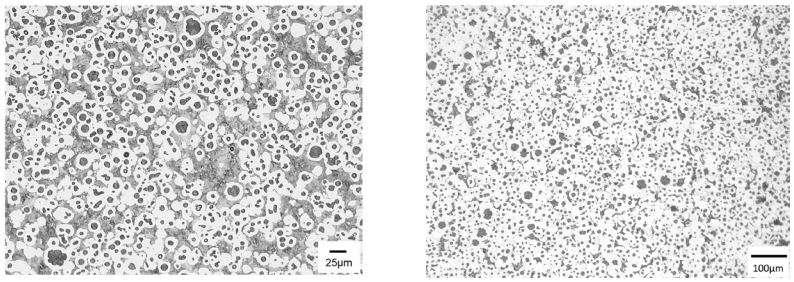

(a) Coin casting (b) Knuckle casting

Figure 6. Microstructures of the coin casting and knuckle casting.

Table 3. Expansion and Contraction Values in Solidification (vol.%)

No.	Molding		Casting		Liquid contraction	Primary austenite contraction or graphite expansion	In eutectic solidification		Austenite contraction in eutectic cells	Volume change from pouring to completion of solidification
	Type	Material	Modulus	Shape			Austenite contraction	Graphite expansion		
1	Furan	Artificial sand	10cm	Cube	-2.10	0.00	-3.28	6.27	-0.09	0.81
2	Furan	Silica sand	10cm	Cube	-0.70	-0.47	-3.33	6.42	-0.01	1.91
3	Green	Silica sand	1cm	Cube	-2.07	-0.14	-3.10	0.00	-0.26	-5.58
4				Flat						
5	PM	SAE1049	0.3cm	Coin	-2.15	0.85	-3.05	0.00	-0.31	-4.66
6			3cm	Knuckle	-1.58	0.85	-3.23	5.83	-0.14	1.72

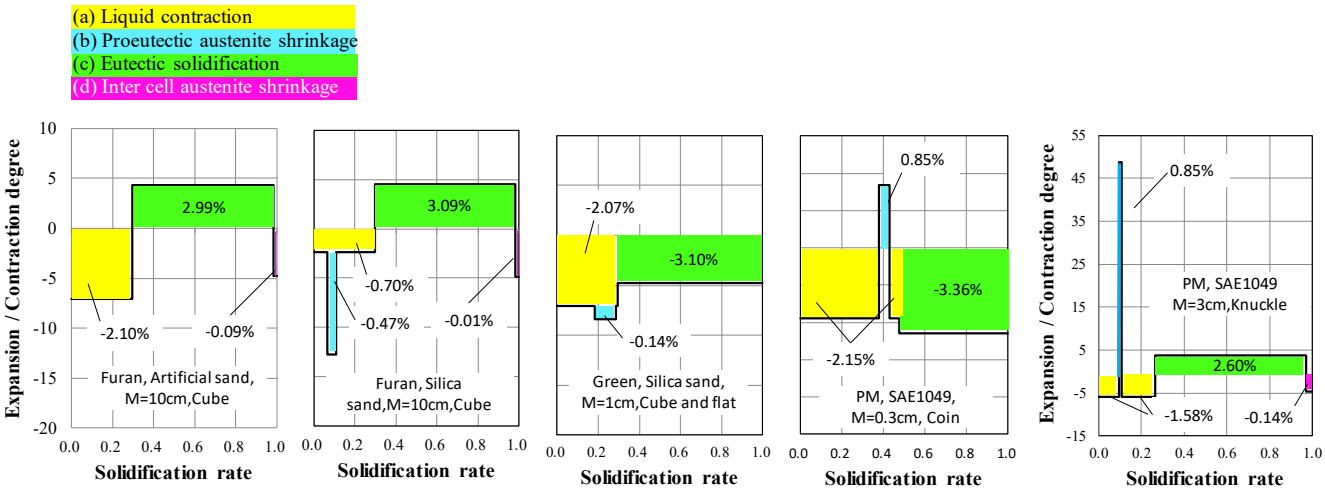

Figure 7. Expansion and solidification behavior of the castings

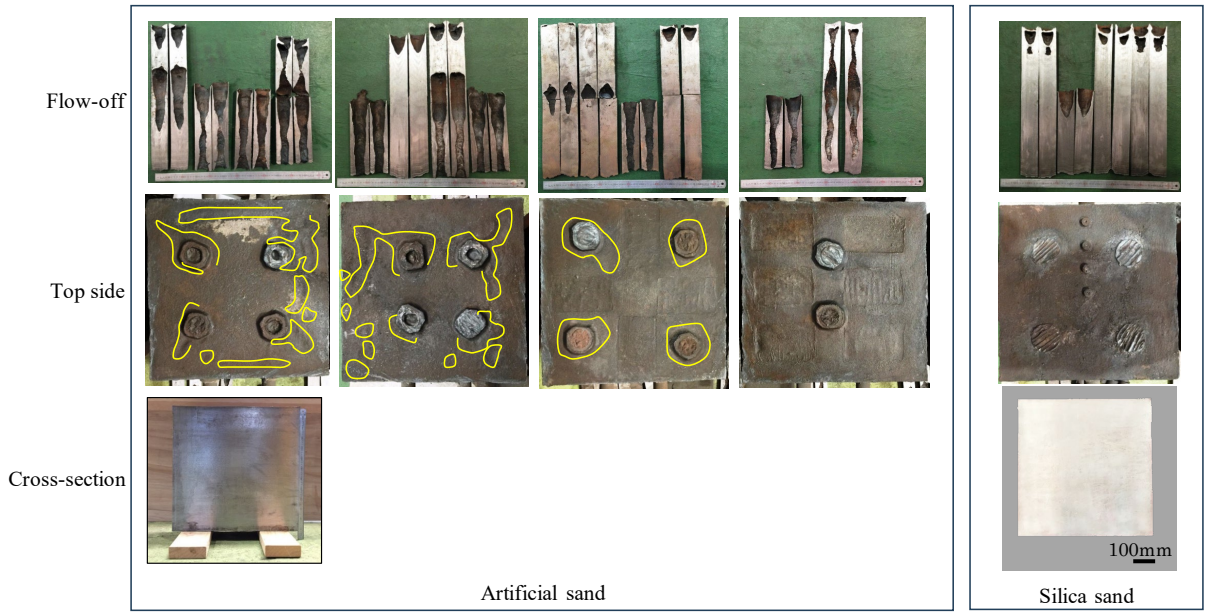

Figure 8. Large cubic shape casting results for molds using artificial sand and silica sand.

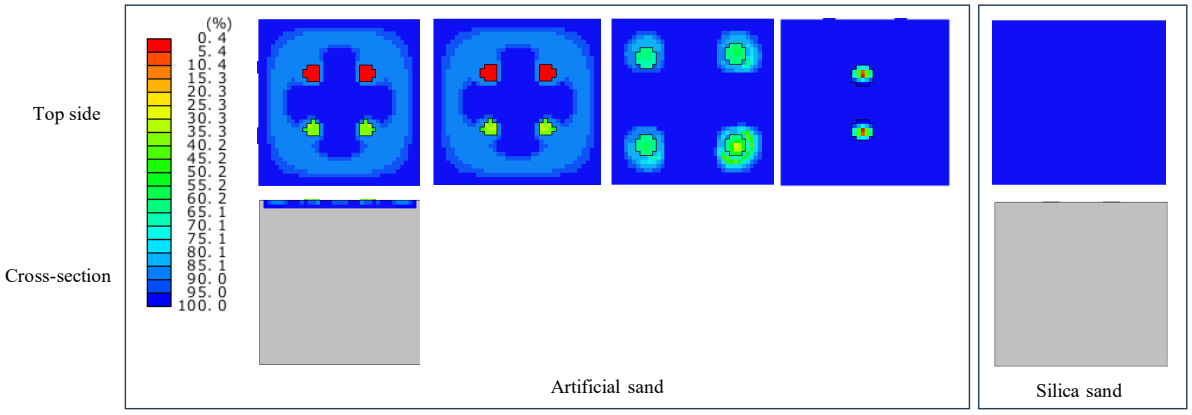

(a) This study method

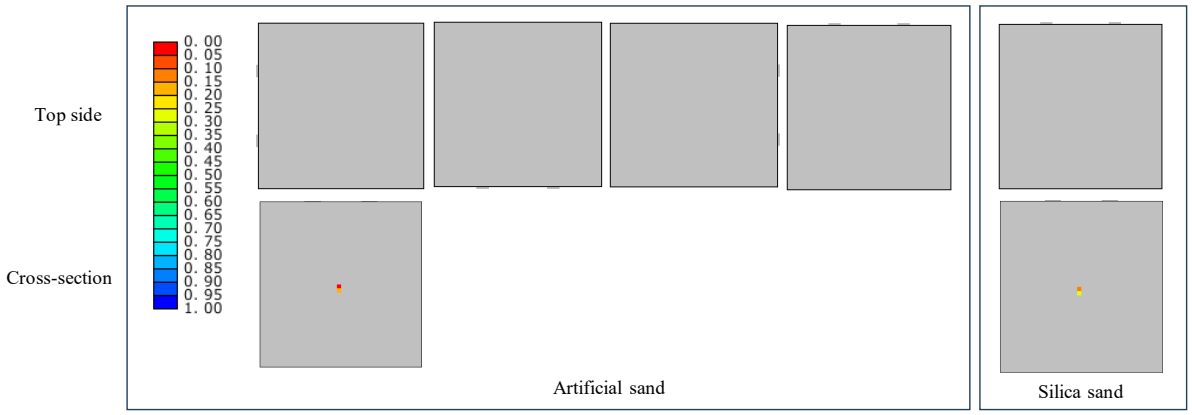

(b) Niiyama criterion as conventional method

Figure 9. Shrinkage prediction results of large cubic shape castings.

Small cubic and flat shape castings using green sand molding with silica sand

Figure 10 shows the appearance and cross-section of the casting. External and internal shrinkages were observed in castings made with green sand molds. Table 4 shows the dimensional measurements of the castings, revealing that the dimensions of the green sand castings were larger than those of the wooden models. This suggests that the pressure caused by eutectic expansion during solidification pushed the mold apart. Figure 11 shows the predicted results of the shrinkage cavity, indicating that the green sand molds exhibited shrinkage cavities similar to those of the actual castings. The shrinkage cavity distribution was more accurate when the mold characteristics were considered.

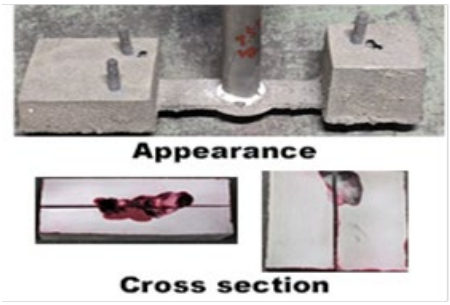

Figure 10. Appearance and section of the castings with a green sand mold.

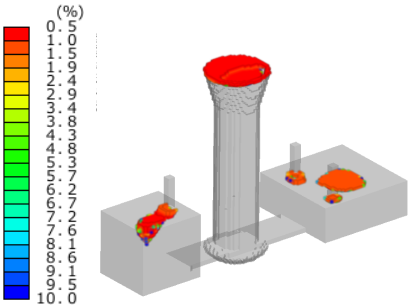

(a) This study method

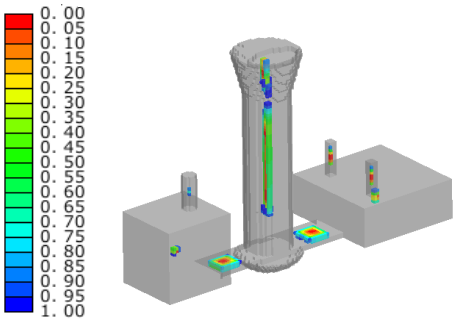

(b) Niiyama criterion as conventional method

Figure 11. Prediction results of the shrinkage cavity for green sand mold casting.

Table 4. Dimensional Measurements for Small Cubic and Flat Castings

Mesurement section			Cubic casting			
			Wooden model (mm)	Green sand mold		
				Casting (mm)	Shrinkage rate	
					Each	Ave.
Width	Front	a) Top	70	70.1	0.1%	2.76%
		b) Mid.	71	73.0	2.8%	
		c) Bot.	72	73.7	2.4%	
	Back	a)	70	70.4	0.6%	
		b)	71	72.9	2.7%	
		c)	72	74.7	3.8%	
	Left	a)	70	70.9	1.3%	
		b)	71	74.0	4.2%	
		c)	72	76.3	6.0%	
	Right	a)	70	72.2	3.1%	
		b)	71	73.7	3.8%	
		c)	72	73.7	2.4%	
Thickness		1	70	70.0	0.0%	0.45%
		2		70.2	0.3%	
		3		70.4	0.6%	
		4		70.6	0.9%	
		5		70.0	0.0%	
		6		70.4	0.6%	
		7		70.4	0.6%	
		8		70.5	0.7%	

Mesurement section			Flat casting			
			Wooden model (mm)	Green sand mold		
				Casting (mm)	Shrinkage rate	
					Each	Ave.
Width	Front	a) Top	99	100.4	1.4%	1.77%
		b) Mid.	100	101.2	1.2%	
		c) Bot.	101	103.6	2.6%	
	Back	a)	99	100.7	1.7%	
		b)	100	101.2	1.2%	
		c)	101	102.8	1.8%	
	Left	a)	99	100.7	1.7%	
		b)	100	101.9	1.9%	
		c)	101	103.2	2.2%	
	Right	a)	99	100.4	1.4%	
		b)	100	101.6	1.6%	
		c)	101	103.6	2.6%	
Thickness		1	40	40.5	1.3%	1.03%
		2		41.0	2.5%	
		3		40.0	0.0%	
		4		40.2	0.5%	
		5		40.8	2.0%	
		6		40.4	1.0%	
		7		40.0	0.0%	
		8		40.4	1.0%	

Coin shape or steering knuckle castings with permanent mold

Figure 12 shows the permanent mold castings. The coin casting exhibited a shrinkage cavity, while the steering knuckle casting, upon being cut and inspected, showed no signs of shrinkage cavities in cut sections. Figure 13 shows the predicted results of the shrinkage cavity, indicating that the distribution closely matched the actual shrinkage cavity distribution.

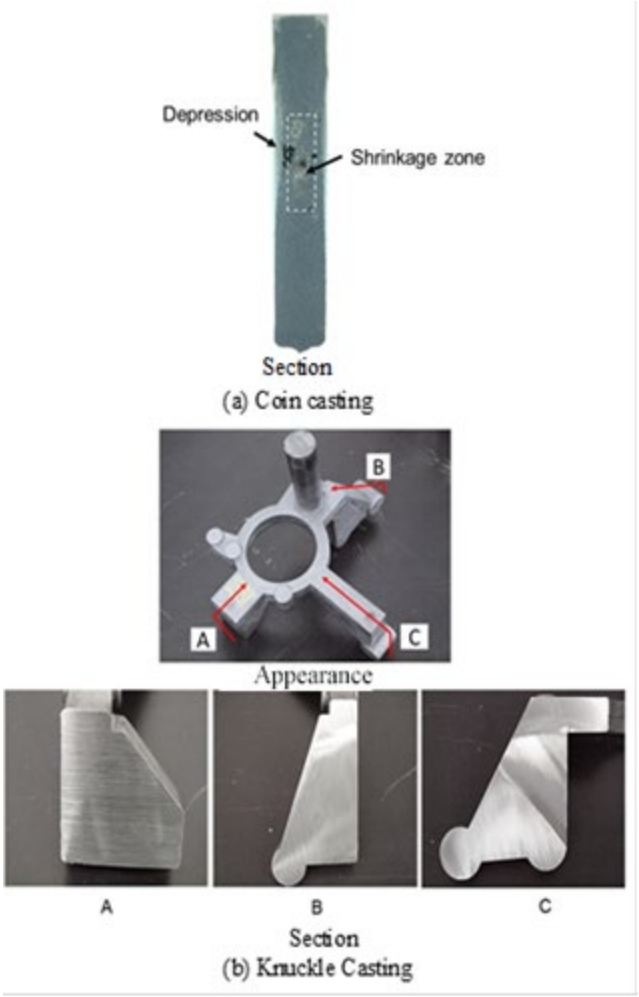

Figure 12. Appearance and section of the PM castings.

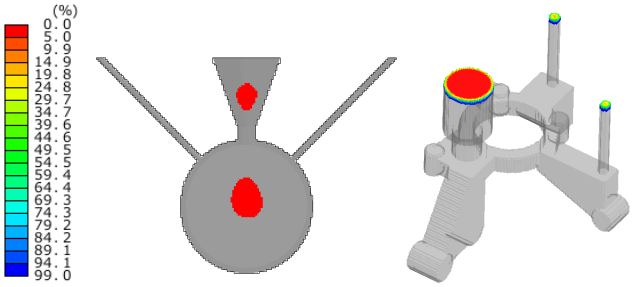

(a) This study method

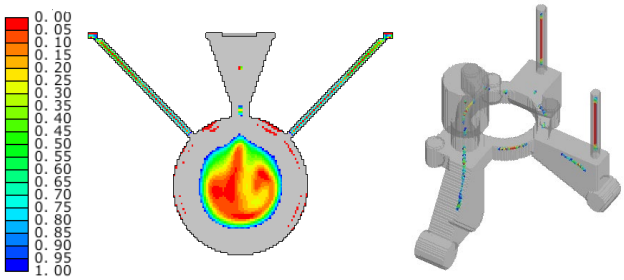

(b) Niiyama criterion as conventional method

Figure 13. Shrinkage cavity prediction result of PM castings.

CONCLUSION

The possibility of improving the accuracy of shrinkage cavity prediction in casting simulations was found by incorporating expansion and contraction behavior during solidification, considering mold characteristics such as mold aggregate, process, size, and shape.

1. For molds with a large thermal expansion coefficient, such as furan process silica sand molds, the external shrinkage cavity distribution can be made closer to the actual distribution by subtracting the thermal expansion coefficient of the silica sand from the liquid shrinkage rate.
2. For molds with low strength, such as green sand molds, the shrinkage cavity distribution can be made closer to the actual distribution by reducing the value of eutectic expansion.
3. For permanent molds, the shrinkage cavity distribution can be made closer to the actual distribution by setting the value of eutectic expansion to zero when the casting modulus is small.

To further improve shrinkage cavity prediction, casting tests with several stable variables are needed to validate the results, which will be the subject of our next study.

REFERENCES

1. Miyamoto, Y., Itofuji, H., “Shrinkage Analysis Considering Expansion and Contraction Behavior in Heavy-Section Spheroidal Graphite Iron Castings,” *AFS Transactions,* pp. 243ff (2019)
2. Chang, B., Akechi, K., Hnawa, K., “Spheroidal Graphite Cast Iron Basis,” *Theory, Practice* (1983).
3. Tsumura, O., Tomigashi, D., Narita, H., Okino, M., Miyauchi, K., “Influence of Low Thermal Expansion Ratio of Artificial Sand Mold on Open Shrinkage of DCI,” *Journal of Japan Foundry Engineering Society,* vol. 81 (7), pp.337ff (2009).
4 Tanaka, T., “Relation between Shape of External Shrinkage Defect and Solidification Expansion Curve for Spheroidal Graphite Iron Castings,” *Imono* vol.42 (8), pp.610ff (1969).
5. Itofuji,H., Edane, K., Sakatani, T., Utagawa, N., Itamura, M.,“PM and Rheocasting In Ductile Iron Castings,” *International Journal of Metalcasting,* (Published online: 12 May 2024).
6. Karsay, S.I., “Ductile Iron I-Production,” *Quebec Iron and Titanium* (1992).
7. Chang, B., “The Riserless Design of Ductile Cast Iron,” *Imono*, vol. 55 pp. 113ff (1983).
8. Su, K., Ohnaka, I., Yamauchi, I., Fukusako, T., “Volumetric Change of Columnar Spheroidal Graphite Iron Castings during Solidification,” *Journal of Japan Foundry Engineering Society,* vol. 58 (10), pp.702ff (1986).
9. Yoshida, T., Kawabata, M., “Evaluation of Shrinkage Tendency of Spheroidal Graphite Cast Iron,” *Journal of Japan Foundry Engineering Society,* vol. 70 (5), pp.336ff (1998).
10. Hoched, B., at al., *Diagrammes d'équilibre-Alliages terniaires* (1978).